J. Approx. Softw., Vol. 1, No. 2 (2024) 3

Journal of Approximation Software

Exponential integrators for a mean-field selective optimal control problem

G. Albi [1], M. Caliari [1,⋆], E. Calzola [1], and F. Cassini [1]

[1] *Department of Computer Science, University of Verona, Italy*

Received: 04/07/2024 – Published: 06/09/2024
Communicated by: M. Vianello

Dedicated to Professor Leonard Peter Bos on the occasion of his 70th birthday

Abstract

In this paper we consider a mean-field optimal control problem with selective action of the control, where the constraint is a continuity equation involving a non-local term and diffusion. First order optimality conditions are formally derived in a general framework, accounting for boundary conditions. Hence, the optimality system is used to construct a reduced gradient method, where we introduce a novel algorithm for the numerical realization of the forward and the backward equations, based on exponential integrators. We illustrate extensive numerical experiments on different control problems for collective motion in the context of opinion formation, pedestrian dynamics, and mass transfer.

Keywords: mean-field control, multi-agent systems, PDE-constrained optimization, exponential integrators (MSC2020: 65M22, 49M41, 93A16)

1 Introduction

The study of collective motion of interacting agents systems is of paramount importance to understand the formation of coherent global behaviors at various scales, with applications to the study of biological, social, and economic phenomena. In recent years, there has been a surge of literature on the collective behavior of multi-agent systems, covering a wide range of topics such as cell aggregation and motility, coordinated animal motion [28, 30], opinion formation [36, 45, 55], coordinated human behavior [10, 27, 31, 48], and cooperative robots [26, 34, 46, 47]. These fields are vast and constantly evolving and we refer to the surveys [8, 29, 39] that provide a comprehensive overview of recent developments. Modeling such complex and diverse systems poses a significant challenge, since in general there are no first-principles

⋆ Corresponding author: marco.caliari@univr.it

as, for instance, in classical physics, or statistical mechanics. Nevertheless, the dynamics of the individuals have been successfully described by systems of Ordinary Differential Equations (ODEs) from Newton's laws designing basic interaction rules, such as attraction, repulsion, and alignments, or, alternatively, by considering an evolutive game where the dynamics is driven by the simultaneous optimization of costs by N players such as in References [42, 43]. In this context, of paramount importance for several applications is the design of centralized policies able to optimally enforce a desired state of the agents, see for instance References [5, 6, 23].

In this paper, we consider a constrained setting, where interacting individuals are influenced by a centralized control with selective action, i.e.,

$$\mathrm{d}x_i = \left(\frac{1}{N} \sum_{j=1}^{N} p(x_i, x_j)(x_j - x_i) + s(t, x_i, \rho^N) u_i \right) \mathrm{d}t + \sigma \mathrm{d}W_i^t, \tag{1}$$

with initial data $x^0 = [x_1^0, \dots, x_N^0]$. Here, each agent $x_i \in \Omega \subseteq \mathbb{R}^d$, for $i = 1, \dots, N$, accounts for pairwise interactions weighted by the function $p(\cdot,\cdot)$, and for disturbances modelled with a Brownian motion $\mathrm{d}W_i^t$. The action of the control $u = [u_1, \dots, u_N]$, $u_i \in \mathbb{R}^d$, is weighted by a selective function $s(t, x_i, \rho^N)$, with $\rho^N(x)$ the empirical measures associated to the interacting agent system, i.e., $\rho^N(t,x) = N^{-1} \sum_{i=1}^{N} \delta(x_i(t) - x)$. Then, the optimal control is obtained by minimizing the cost functional

$$J(u; x^0) = \mathbb{E}\left[\int_0^T \frac{1}{2N} \sum_{i=1}^{N} \left(\ell(t, x_i, \rho^N) + \gamma |u_i|^2 \right) \right], \tag{2}$$

where $\ell(t, x_i, f^N)$ is a running cost to be designed by the controller, with a quadratic penalization of the control for $\gamma \geq 0$.

For a large number of agents, we can write the mean-field optimal control problem corresponding to the finite dimensional optimal control problem (1)–(2) as follows (see References [11, 32, 33])

$$\min_{u \in U} \frac{1}{2} \int_0^T \int_\Omega \left(\ell(t, x, \rho) + \gamma |u|^2 \right) \rho \, dx dt. \tag{3a}$$

Here, U is the space of admissible controls and ρ is the density function satisfying the Partial Differential Equation (PDE)

$$\begin{cases} \partial_t \rho + \nabla \cdot \left(\left(\mathscr{P}(\rho) + s(t, x, \rho) u \right) \rho \right) - \dfrac{\sigma^2}{2} \Delta \rho = 0, \\ \rho(0, x) = \rho_0(x). \end{cases} \tag{3b}$$

The non-local interactions among agents are described by the integral term

$$\mathscr{P}(\rho)(t, x) = \int_\Omega p(x, y)(y - x) \rho(t, y) dy \tag{4}$$

and $\rho_0(x)$ is the initial distribution of the agents. Differently from mean-field games [1, 22, 43], in this context the goal is to compute a mean-field optimal strategy capable of driving the population density to a specific target, avoiding the curse of dimensionality induced by the large scale non-linear system of N agents. However, the numerical solution of the PDE-constrained optimization problem (3a)–(3b) requires careful treatment, see Reference [15]. In mean-field optimal control problems, various methodologies have been utilized to tackle the synthesis of high-dimensional systems, as seen in References [2, 24, 33, 49]. In this study, we adopt a

reduced gradient method strategy where the first order optimality system is solved iteratively for the realization of the control, as in References [7, 12]. Major challenges arise from the presence of the stiff diffusive and transport operators, and from the stability and storage requirements originated by the choice of the numerical solvers. For these kinds of problems, explicit time marching schemes usually require several time steps due to the lack of favorable stability properties, while implicit ones need possibly expensive solutions of non-linear systems (see References [9, 37], where implicit multistep or Runge–Kutta methods are employed) or linear systems (see Reference [40], where IMEX methods are proposed). A prominent and effective alternative way to numerically integrate stiff equations in time is to employ explicit *exponential integrators*, see Reference [41] for a seminal review. After semidiscretization in space, these schemes require to approximate the action of exponential and of exponential-like matrix functions (the so-called φ-functions), in contrast to the solution of (non-)linear systems.

The paper is structured as follows. In Section 2 we present a model of interest which generalizes the one in formulas (3), and we derive the formal optimality conditions using the associated Lagrangian function, obtaining a system of coupled PDEs. The first one is forward in time for the density function, while the second is backward in time for the adjoint variable. We numerically couple these equations using the steepest descent algorithm. In Section 3 we present the semidiscretization in space of the forward and of the backward PDEs, together with the numerical solution of the arising systems of ODEs using a pair of exponential integrators. For convenience of the reader, we also present there the derivation of the schemes and a brief discussion on common techniques to compute the involved matrix functions. Section 4 is devoted to some numerical validations and simulations in opinion formation (Sznajd, Hegselmann–Krause, and mass transfer) and pedestrian (see Reference [16]) models. We finally draw some conclusions in Section 5.

2 Mean-field selective optimal control problem

We consider the mean-field optimal control problem [7, 16, 32] defined by the functional minimization

$$\min_{u\in U} \mathscr{J}(u;\rho_0), \tag{5a}$$

where $\rho = \rho(t,x) \in \mathbb{R}$ is a probability density of agents satisfying

$$\begin{cases} \partial_t \rho + \nabla\cdot\left[\left(\mathscr{P}(\rho) + s(t,x,\rho)u\right)\rho\right] - \dfrac{\sigma^2}{2}\Delta\rho = 0, \\ \rho(0,x) = \rho_0(x), \\ \left(\left(\mathscr{P}(\rho) + s(t,x,\rho)u\right)\rho - \dfrac{\sigma^2}{2}\nabla\rho\right)\cdot\vec{n} = \begin{cases} \beta\rho & \text{on } \Gamma_F, \\ 0 & \text{on } \Gamma_Z \end{cases} \end{cases} \tag{5b}$$

and defined for each $(t,x) \in [0,T]\times\Omega$. The evolution of the density is driven by the non-local operator $\mathscr{P}(\rho)(t,x) \in \mathbb{R}^d$, as in equation (4), and by the control $u = u(t,x) \in \mathbb{R}^d$ weighted by the selective function $s(t,x,\rho) \in \mathbb{R}$. Here, we denoted by Γ_F the subset of the boundary in which there is a flux different from zero ($\beta \neq 0$) and by Γ_Z the part of $\partial\Omega$ with zero-flux boundary conditions. These two subsets are such that $\Gamma_F \cup \Gamma_Z = \partial\Omega$ and $\Gamma_F \cap \Gamma_Z = \emptyset$, and $\vec{n}$ is the outward normal vector to the boundary with norm equal to one. Finally, the functional in formula (5a) is given by

$$\mathscr{J}(u;\rho_0) = \frac{1}{2}\int_0^T \int_\Omega \left(e(t,x,\rho) + \gamma|u|^2\rho\right) dxdt + \frac{1}{2}\int_\Omega c(T,x,\rho(T,x))dx$$

for a general running cost $e(t,x,\rho) \in \mathbb{R}$ and a terminal cost $c(T,x,\rho(T,x)) \in \mathbb{R}$.

2.1 First order optimality conditions

We can derive the first order optimality conditions on a formal level using a Lagrangian approach. For a rigorous treatment we refer to References [7, 17]. We define the Lagrangian function with adjoint variable ψ as

$$\begin{aligned}\mathscr{L}(u,\rho,\psi) =& \frac{1}{2}\int_0^T \int_\Omega \left(e(t,x,\rho) + \gamma|u|^2\rho\right) dxdt + \frac{1}{2}\int_\Omega c(T,x,\rho(T,x))dx \\ &- \int_0^T \int_\Omega \psi \left(\partial_t\rho + \nabla\cdot\left[\left(\mathscr{P}(\rho) + s(t,x,\rho)u\right)\rho\right] - \frac{\sigma^2}{2}\Delta\rho\right) dxdt.\end{aligned} \tag{6}$$

The optimal solution (u^*,ρ^*,ψ^*) can be found by equating to zero the partial Fréchet derivatives of the Lagrangian function, i.e., by solving the following system

$$\begin{cases} D_u\mathscr{L}(u,\rho,\psi) = 0, \\ D_\psi\mathscr{L}(u,\rho,\psi) = 0, \\ D_\rho\mathscr{L}(u,\rho,\psi) = 0. \end{cases} \tag{7}$$

Before computing the partial derivatives in system (7), we integrate by parts the last term appearing in the Lagrangian function (6) and we get

$$\begin{aligned}\mathscr{L}(u,\rho,\psi) =& \frac{1}{2}\int_0^T \int_\Omega \left(e(t,x,\rho) + \gamma|u|^2\rho\right) dxdt + \frac{1}{2}\int_\Omega c(T,x,\rho(T,x))dx \\ &+ \int_0^T \int_\Omega \rho \left(\partial_t\psi + \frac{\sigma^2}{2}\Delta\psi + \left(\mathscr{P}(\rho) + s(t,x,\rho)u\right)\cdot\nabla\psi\right) dxdt \\ &- \int_0^T \int_{\Gamma_F} \rho \left(\frac{\sigma^2}{2}\nabla\psi\cdot\vec{n} + \beta\psi\right) dbdt \\ &- \int_\Omega (\psi(T,x)\rho(T,x) - \psi(0,x)\rho(0,x))dx,\end{aligned}$$

where we used the value of the boundary conditions appearing in equation (5b). Performing then the computations of the partial derivatives we obtain the gradient direction for the control variable u

$$D_u\mathscr{L}(u,\rho,\psi) = \gamma u + s(t,x,\rho)\nabla\psi, \tag{8}$$

the forward PDE for the density function ρ

$$\begin{cases} \partial_t\rho + \nabla\cdot\left[\left(\mathscr{P}(\rho) + s(t,x,\rho)u\right)\rho\right] - \dfrac{\sigma^2}{2}\Delta\rho = 0, \\ \rho(0,x) = \rho_0(x), \\ \left(\left(\mathscr{P}(\rho) + s(t,x,\rho)u\right)\rho - \dfrac{\sigma^2}{2}\nabla\rho\right)\cdot\vec{n} = \begin{cases}\beta\rho & \text{on } \Gamma_F, \\ 0 & \text{on } \Gamma_Z,\end{cases} \end{cases} \tag{9}$$

and the backward PDE for the adjoint variable ψ

$$\begin{cases} -\partial_t \psi = \dfrac{\sigma^2}{2}\Delta\psi + \big(\mathscr{P}(\rho) + (s(t,x,\rho) + \rho D_\rho s(t,x,\rho))u\big)\cdot\nabla\psi \\ \qquad\qquad + \mathscr{Q}(\rho,\psi) + \dfrac{1}{2}(D_\rho e(t,x,\rho) + \gamma|u|^2), \\ \psi(T,x) = \psi_T(x), \\ \dfrac{\sigma^2}{2}\nabla\psi\cdot\vec{n} = \begin{cases} -\beta\psi & \text{on } \Gamma_{\mathrm{F}}, \\ 0 & \text{on } \Gamma_{\mathrm{Z}}, \end{cases} \end{cases} \tag{10}$$

where

$$\mathscr{Q}(\rho,\psi)(t,x) = \int_\Omega p(y,x)(x-y)\cdot\nabla\psi(t,y)\rho(t,y)dy$$

and $\psi_T(x) = \frac{1}{2}D_\rho c(T,x,\rho(T,x))$. Now, in order to solve model (5), we employ a steepest descent approach (see References [7, 12]). Starting with an initial control u^0, at each iteration ℓ we insert u^ℓ into the forward equation (9) and solve it for $\rho = \rho^{\ell+1}$. We then insert u^ℓ and $\rho^{\ell+1}$ into the backward equation (10) and solve it for $\psi = \psi^{\ell+1}$. We finally update the control by using the gradient direction (8), i.e.,

$$u^{\ell+1} = u^\ell - \lambda^\ell(\gamma u^\ell + s(t,x,\rho^{\ell+1})\nabla\psi^{\ell+1})$$

and get $u^{\ell+1}$. We proceed iterating until $\mathscr{J}(u^{\ell+1})$ has stabilized within a given tolerance. For the numerical solution of equations (9) and (10) we use the method of lines: we first discretize in space and then use appropriate integrators for the obtained systems of ODEs.

3 Numerical integrators for the semidiscretized equations

In this section, we explain how to solve the forward and the backward PDEs in the steepest descent algorithm. By observing that both are semilinear parabolic equations, the idea is to use numerical schemes tailored for this type of problems. A prominent way is to apply explicit exponential integrators [41] to the systems of ODEs arising from the semidiscretization in space of the PDEs. By construction, these schemes solve exactly linear ODEs systems with constant coefficients and they allow for time steps usually much larger than those required by classical explicit methods, i.e., typically they do not suffer from a CFL restriction. On the other hand, this class of integrators requires the computation of the action of exponential-like matrix functions for which different efficient techniques have been developed in recent years (see Section 3.3).

3.1 Forward PDE

For the sake of clarity, and since we will present later on one-dimensional numerical examples, we consider $\Omega = [a,b]$ and we rewrite the forward PDE (9)

$$\begin{cases} \partial_t \rho(t,x) = \dfrac{\sigma^2}{2}\partial_{xx}\rho(t,x) - \partial_x\left((\mathscr{P}(\rho(t,\cdot))(t,x) + s(t,x,\rho(t,x))u(t,x))\rho(t,x)\right), \\ \rho(0,x) = \rho_0(x), \\ \left((\mathscr{P}(\rho(t,\cdot))(t,x) + s(t,x,\rho(t,x))u(t,x))\rho(t,x) - \dfrac{\sigma^2}{2}\partial_x\rho(t,x)\right)\Big|_a = \beta_a\rho(t,a), \\ \left((\mathscr{P}(\rho(t,\cdot))(t,x) + s(t,x,\rho(t,x))u(t,x))\rho(t,x) - \dfrac{\sigma^2}{2}\partial_x\rho(t,x)\right)\Big|_b = \beta_b\rho(t,b), \end{cases}$$

where $\beta_a, \beta_b \in \mathbb{R}$ can be selected so that it is possible to express both zero and nonzero fluxes. Notice that when we solve this equation we consider $u(t,x)$ a given function. We introduce a semidiscretization in space by finite differences on a grid of points x_i, with $i = 1,\dots,n$, in such a way that $\boldsymbol{\rho}(t) = [\rho_1(t),\dots,\rho_n(t)]^\mathsf{T}$ is the unknown vector whose components $\rho_i(t)$ approximate $\rho(t,x_i)$. Now, by denoting D_1 and D_2 the matrices which discretize ∂_x and ∂_{xx} at the grid points, respectively, and P the discretization of the linear integral operator $\mathscr{P}$ by a quadrature formula, the linear part of the right hand side of the equation is discretized by

$$\frac{\sigma^2}{2}D_2\boldsymbol{\rho}(t),$$

while the non-linear part becomes

$$\begin{aligned} &-(D_1P\boldsymbol{\rho}(t))\boldsymbol{\rho}(t) - (P\boldsymbol{\rho}(t))(D_1\boldsymbol{\rho}(t)) \\ &\qquad - (D_1\boldsymbol{s}(t,\boldsymbol{\rho}(t)))\boldsymbol{u}(t)\boldsymbol{\rho}(t) - \boldsymbol{s}(t,\boldsymbol{\rho}(t))(D_1\boldsymbol{u}(t))\boldsymbol{\rho}(t) - \boldsymbol{s}(t,\boldsymbol{\rho}(t))\boldsymbol{u}(t)(D_1\boldsymbol{\rho}(t)). \end{aligned}$$

Now, we also discretize the boundary conditions with finite differences by using virtual nodes, and we modify accordingly both the linear part and the non-linear one. The resulting non-linear system of ODEs is then

$$\begin{cases} \boldsymbol{\rho}'(t) = A_\mathrm{F}\boldsymbol{\rho}(t) + \boldsymbol{g}_\mathrm{F}(t,\boldsymbol{\rho}(t)), \quad t \in [0,T], \\ \boldsymbol{\rho}(0) = \boldsymbol{\rho}_0. \end{cases} \tag{11}$$

Given a time discretization $[t_0,\dots,t_k,\dots,t_m]$, with $t_0 = 0$ and $t_m = T$, the exact solution of system (11) at time t_{k+1} can be expressed using the variation-of-constants formula, i.e.,

$$\boldsymbol{\rho}(t_{k+1}) = \mathrm{e}^{\tau_k A_\mathrm{F}}\boldsymbol{\rho}(t_k) + \int_0^{\tau_k} \mathrm{e}^{(\tau_k - s)A_\mathrm{F}}\boldsymbol{g}_\mathrm{F}(t_k + s, \boldsymbol{\rho}(t_k + s))ds,$$

where $\tau_k = t_{k+1} - t_k$, for $k = 0,\dots,m-1$. In order to obtain an explicit first order numerical scheme, we denote by $\boldsymbol{\rho}_k$ the approximation of $\boldsymbol{\rho}(t_k)$ and approximate the non-linear function $\boldsymbol{g}_\mathrm{F}(t_k + s, \boldsymbol{\rho}(t_k + s))$ with $\boldsymbol{g}_\mathrm{F}(t_k, \boldsymbol{\rho}_k)$. Hence, we have

$$\begin{aligned} \boldsymbol{\rho}(t_{k+1}) \approx \boldsymbol{\rho}_{k+1} &= \mathrm{e}^{\tau_k A_\mathrm{F}}\boldsymbol{\rho}_k + \int_0^{\tau_k} \mathrm{e}^{(\tau_k - s)A_\mathrm{F}}\boldsymbol{g}_\mathrm{F}(t_k, \boldsymbol{\rho}_k)ds \\ &= \mathrm{e}^{\tau_k A_\mathrm{F}}\boldsymbol{\rho}_k + \left(\int_0^{\tau_k} \mathrm{e}^{(\tau_k - s)A_\mathrm{F}}ds\right)\boldsymbol{g}_\mathrm{F}(t_k, \boldsymbol{\rho}_k) \\ &= \mathrm{e}^{\tau_k A_\mathrm{F}}\boldsymbol{\rho}_k + \left(\tau_k\int_0^1 \mathrm{e}^{\tau_k(1-\theta)A_\mathrm{F}}d\theta\right)\boldsymbol{g}_\mathrm{F}(t_k, \boldsymbol{\rho}_k) \\ &= \mathrm{e}^{\tau_k A_\mathrm{F}}\boldsymbol{\rho}_k + \tau_k\varphi_1(\tau_k A_\mathrm{F})\boldsymbol{g}_\mathrm{F}(t_k, \boldsymbol{\rho}_k). \end{aligned} \tag{12}$$

Here, we introduced the exponential-like function

$$\varphi_1(X) = \int_0^1 \mathrm{e}^{(1-\theta)X} d\theta,$$

with $X \in \mathbb{C}^{n\times n}$ a generic matrix. This scheme is known as *exponential Euler*, it is an explicit method of first (stiff) order and it is A-stable by construction. Although its implementation does not need the solution of (non-)linear systems, at each time step it is required the evaluation of a linear combination of type $\mathrm{e}^{\tau_k X}\boldsymbol{v}_k + \tau_k\varphi_1(\tau_k X)\boldsymbol{w}_k$, where $\boldsymbol{v}_k, \boldsymbol{w}_k \in \mathbb{C}^n$ are suitable vectors, which we will address in Section 3.3.

3.1.1 Selective function independent of the density

A remarkable occurrence in the literature is $s(t,x,\rho(t,x)) = s(t,x)$, i.e., the selective function does not depend on the density (see Reference [7] for the case $s(t,x) = 1$, which we will also consider in the numerical examples). In this case, the linear part of the forward equation has time dependent coefficients

$$\left(\frac{\sigma^2}{2}D_2 - (D_1\boldsymbol{s}(t))\boldsymbol{u}(t) - \boldsymbol{s}(t)(D_1\boldsymbol{u}(t)) - \boldsymbol{s}(t)\boldsymbol{u}(t)D_1\right)\boldsymbol{\rho}(t),$$

while the non-linear part is now given by

$$-(D_1 P\boldsymbol{\rho}(t))\boldsymbol{\rho}(t) - (P\boldsymbol{\rho}(t))(D_1\boldsymbol{\rho}(t)).$$

By modifying accordingly the quantities to impose the boundary conditions, and using again the previous notation for simplicity, we end up with the system of ODEs

$$\begin{cases} \boldsymbol{\rho}'(t) = A_{\mathrm{F}}(t)\boldsymbol{\rho}(t) + \boldsymbol{g}_{\mathrm{F}}(t,\boldsymbol{\rho}(t)), \quad t \in [0,T], \\ \boldsymbol{\rho}(0) = \boldsymbol{\rho}_0. \end{cases} \tag{13}$$

At each t_k we can rewrite equivalently this system as

$$\begin{cases} \boldsymbol{\rho}'(t) = A_{\mathrm{F}}(t_k)\boldsymbol{\rho}(t) + (A_{\mathrm{F}}(t) - A_{\mathrm{F}}(t_k))\boldsymbol{\rho}(t) + \boldsymbol{g}_{\mathrm{F}}(t,\boldsymbol{\rho}(t)) \\ \qquad\quad = A_{\mathrm{F}}(t_k)\boldsymbol{\rho}(t) + \boldsymbol{g}^k_{\mathrm{F}}(t,\boldsymbol{\rho}(t)), \\ \boldsymbol{\rho}(0) = \boldsymbol{\rho}_0 \end{cases}$$

and apply the exponential Euler method, as done for system (11). Thus, we end up with the scheme

$$\begin{aligned} \boldsymbol{\rho}(t_{k+1}) \approx \boldsymbol{\rho}_{k+1} &= \mathrm{e}^{\tau_k A_{\mathrm{F}}(t_k)}\boldsymbol{\rho}_k + \tau_k\varphi_1(\tau_k A_{\mathrm{F}}(t_k))\boldsymbol{g}^k_{\mathrm{F}}(t_k,\boldsymbol{\rho}_k) \\ &= \mathrm{e}^{\tau_k A_{\mathrm{F}}(t_k)}\boldsymbol{\rho}_k + \tau_k\varphi_1(\tau_k A_{\mathrm{F}}(t_k))\boldsymbol{g}_{\mathrm{F}}(t_k,\boldsymbol{\rho}_k), \end{aligned} \tag{14}$$

for $k = 0,\dots,m-1$. As for the general case $s(t,x,\rho(t,x))$, we obtain in this way an explicit method of first order (which we call *exponential Euler–Magnus*) that requires again to evaluate a linear combination of actions of the matrix exponential and the matrix φ_1 function.

3.2 Backward PDE

We rewrite the backward PDE (10) in the one-dimensional case $\Omega = [a,b]$

$$\begin{cases} -\partial_t \psi(t,x) = \dfrac{\sigma^2}{2}\partial_{xx}\psi(t,x) + \mathscr{P}(\rho(t,\cdot))(t,x)\partial_x\psi(t,x) \\ \qquad\qquad + (s(t,x,\rho(t,x)) + \rho(t,x)s_\rho(t,x,\rho(t,x)))u(t,x)\partial_x\psi(t,x) \\ \qquad\qquad + \mathscr{Q}(\rho(t,\cdot),\psi(t,\cdot))(t,x) + \dfrac{1}{2}\left(e_\rho(t,x,\rho(t,x)) + \gamma u^2(t,x)\right), \\ \psi(T,x) = \psi_T(x), \\ \dfrac{\sigma^2}{2}\partial_x\psi(t,x)\big|_a = -\beta_a\psi(t,a), \\ \dfrac{\sigma^2}{2}\partial_x\psi(t,x)\big|_b = -\beta_b\psi(t,b), \end{cases}$$

where $s_\rho(t,x,\rho(t,x)) = D_\rho s(t,x,\rho(t,x))$ and $e_\rho(t,x,\rho(t,x)) = D_\rho e(t,x,\rho(t,x))$. Here, we assume that $\rho(t,x)$ and $u(t,x)$ are given functions. By applying a finite difference discretization on the same spatial grid as above and defining Q the discretization of the linear integral operator $\mathscr{Q}$, we obtain the time dependent coefficient linear part

$$\left(\frac{\sigma^2}{2}D_2 + P\boldsymbol{\rho}(t)D_1 + (\boldsymbol{s}(t,\boldsymbol{\rho}(t)) + \boldsymbol{\rho}(t)\boldsymbol{s}_{\boldsymbol{\rho}}(t,\boldsymbol{\rho}(t)))\boldsymbol{u}(t)D_1 + Q\boldsymbol{\rho}(t)D_1\right)\boldsymbol{\psi}(t)$$

and the source term

$$\frac{1}{2}\boldsymbol{e}_{\boldsymbol{\rho}}(t,\boldsymbol{\rho}(t)) + \gamma\boldsymbol{u}^2(t).$$

Finally, by taking into consideration boundary conditions, we end up with the inhomogeneous time dependent coefficient linear system of ODEs

$$\begin{cases} -\boldsymbol{\psi}'(t) = A_{\mathrm{B}}(t)\boldsymbol{\psi}(t) + \boldsymbol{g}_{\mathrm{B}}(t), \quad t \in [0,T], \\ \boldsymbol{\psi}(T) = \boldsymbol{\psi}_T. \end{cases} \tag{15}$$

By considering the same time discretization $[t_0,\dots,t_{k+1},\dots,t_m]$ as above, system (15) has a similar structure to system (13). Hence, taking into account that we are marching backward in time, we apply the exponential Euler–Magnus method and we obtain the time marching

$$\boldsymbol{\psi}(t_k) \approx \boldsymbol{\psi}_k = \mathrm{e}^{\tau_k A_{\mathrm{B}}(t_{k+1})}\boldsymbol{\psi}_{k+1} + \tau_k\varphi_1(\tau_k A_{\mathrm{B}}(t_{k+1}))\boldsymbol{g}_{\mathrm{B}}(t_{k+1}), \tag{16}$$

for $k = m-1, m-2, \dots, 0$.

3.3 Matrix functions evaluation

We have introduced two exponential integrators that require the evaluation of

$$\mathrm{e}^{\tau X}\boldsymbol{v} + \tau\varphi_1(\tau X)\boldsymbol{w}, \tag{17}$$

at each time step, where $\tau > 0$, $X \in \mathbb{R}^{n\times n}$, and $\boldsymbol{v},\boldsymbol{w} \in \mathbb{R}^n$. We stress that these quantities depend in general on the current time step, but for simplicity of notation we dropped the subscripts. If we choose a uniform time discretization, i.e., $\tau_k = \tau$, in the exponential Euler scheme (12) we can compute once and for all the matrices $\mathrm{e}^{\tau A_{\mathrm{F}}}$ and $\varphi_1(\tau A_{\mathrm{F}})$ and then multiply by the

corresponding vectors. In this case, for the matrix function approximations the most common techniques are Taylor expansions or Padé rational approximations with scaling and squaring (see, for instance, References [3, 18, 52, 53]). This approach is computationally attractive only for matrices of moderate size, taking into account also that the resulting matrix functions are full even if the original ones were sparse. When employing the exponential Euler–Magnus schemes (14) and (16), we can still pursue this approach. However, since here the matrices change at each time step, we need to recompute the matrix functions every time accordingly. It is also possible to compute linear combination (17) by using a *single* slightly augmented matrix function evaluation. In fact, thanks to [50, Proposition 2.1], we have that the first n rows of

$$\exp\left(\tau\begin{bmatrix} X & \boldsymbol{w} \\ 0\dots 0 & 0 \end{bmatrix}\right)\begin{bmatrix} \boldsymbol{v} \\ 1 \end{bmatrix}$$

coincide with vector (17). This is an attractive choice in a variable step size scenario, in which both the forward and the backward equations could be solved by a single matrix function evaluation at each time step.

When X is a large sized and sparse matrix, it may be convenient to compute directly vector (17) at each time step *without* explicitly computing the matrix exponential. State-of-the-art techniques follow this approach and are based on Krylov methods or direct interpolation polynomial methods (see, for instance, References [4, 20, 35, 44]).

4 Numerical experiments

We present in this section several numerical examples arising from different choices of parameters and functions in the continuous model (5). In particular, we consider numerical experiments for two different classes of multi-agent systems in opinion formation and pedestrian dynamics, and a mass transfer problem. In all cases, we discretize in space with second order centered finite differences and we employ the trapezoidal rule for the quadrature of the integral operators. All the numerical experiments have been performed on an Intel® Core™ i7-10750H CPU with six physical cores and 16GB of RAM, using MATLAB programming language. As a software, we use MathWorks MATLAB® R2022a. In order to compute the needed actions of exponential and φ_1-function, we employ the `kiops` function[1], which is based on the Krylov method and whose underlying algorithm is presented in Reference [35]. The code used for the simulations, accompanied by a detailed description, can be found in a GitHub repository[2]. In particular, it allows to reproduce the figures of all the following numerical experiments.

4.1 Control in opinion dynamics

In this section we consider two models for control of opinion dynamics, namely the Sznajd and the Hegselmann–Krause (bounded confidence) ones, similarly to References [7, 38, 54]. We set both models in the spatial domain $\Omega = [-1,1]$, whose boundaries represent the extremal opinions. The running cost is $e(t,x,\rho) = (x-x_d)^2\rho$ and the selective function $s(t,x,\rho)$ is set to the constant 1 (hence, we use the exponential Euler–Magnus scheme (14) for the forward equation). For both the problems we consider in model (5) zero-flux boundary conditions everywhere and null terminal cost function $c(T,x,\rho(T,x)) = 0$.

[1] https://gitlab.com/stephane.gaudreault/kiops/-/tree/master/, commit 94149844.
[2] https://github.com/cassinif/expint_mfsoc, commit a7b6748.

4.1.1 Sznajd model

In the first numerical experiment we present an example of Sznajd model for opinion formation taken from Reference [7]. In particular, we consider the interaction function $p(x,y) = x^2 - 1$, representing a repulsive interaction, and the target point in the running cost $x_d = -0.5$. Moreover, we set the penalization parameter $\gamma = 0.5$ and the diffusion coefficient $\sigma = \sqrt{0.02}$. The initial density function is of bimodal type

$$\rho_0(x) = C(\rho_+(x+0.75;0.05,0.5) + \rho_+(x-0.5;0.15,1)),$$

where

$$\rho_+(x;a,b) = \max\left\{-\left(\frac{x}{b}\right)^2 + a, 0\right\}$$

and C defined so that $\int_\Omega \rho_0(x)dx = 1$.

First of all, we show that the expected temporal rate of convergence of the exponential integrators is preserved also after a complete solution of the model. In fact, for a semidiscretization in space with $n = 200$ uniform grid points, we solve several times model (5) by the steepest descent method described at the end of Section 2 by employing an increasing sequence of time steps, ranging from $m = 300$ to $m = 700$. Each time, after the stabilization of the functional $\mathscr{J}$, we measure the error at the final time $T = 4$ for $\boldsymbol{\rho}(t)$ and at initial time for $\boldsymbol{\psi}(t)$ with respect to reference solutions. We display in Figure 1 the obtained relative errors, which confirm the expected accuracy and rate of convergence.

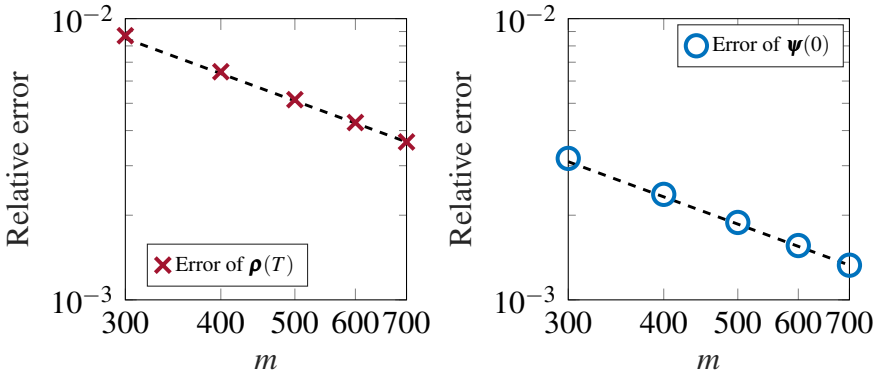

Figure 1: Relative errors in the infinity norm of $\boldsymbol{\rho}(T)$ ($T = 4$, left plot) and $\boldsymbol{\psi}(0)$ (right plot), with respect to a reference solution, for the Sznajd model described in Section 4.1.1 with $n = 200$ spatial discretization points and varying number of time steps m. A black dashed reference line of slope -1 is also displayed.

Then, we show the behavior of the Sznajd model in opinion formation. For this purpose we use a spatial discretization of $n = 800$ points and $m = 200$ time steps. Notice that we decide to employ a relatively large number of discretization points in space to highlight the fact that the exponential integrators do not exhibit any CFL restriction, in contrast to standard explicit methods. In Figures 2 and 3 we show the evolution of the density $\rho(t,x)$ and of the control $u(t,x)$. The results have the expected behavior of concentration of the opinions around the target point $x_d = -0.5$ and qualitatively match the analogous simulation available in the literature [7]. Moreover, we show in Figure 4 the value of the functional $\mathscr{J}(u^\ell)$ at the successive iterations of the steepest descent method. We observe that the method needs 23 iterations to reach the input tolerance $2 \cdot 10^{-3}$. Finally, the overall computational time of this simulation is about 40 seconds.

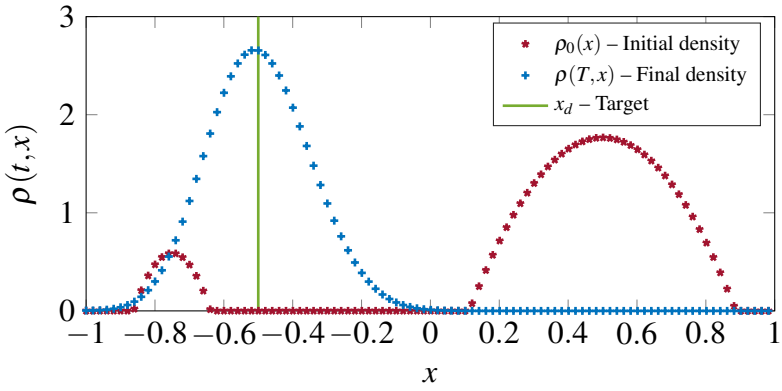

Figure 2: Density functions at initial time and at final time for the Sznajd model described in Section 4.1.1 with $n = 800$ spatial discretization points and $m = 200$ time steps. For visualization reasons, the densities are displayed each tenth point.

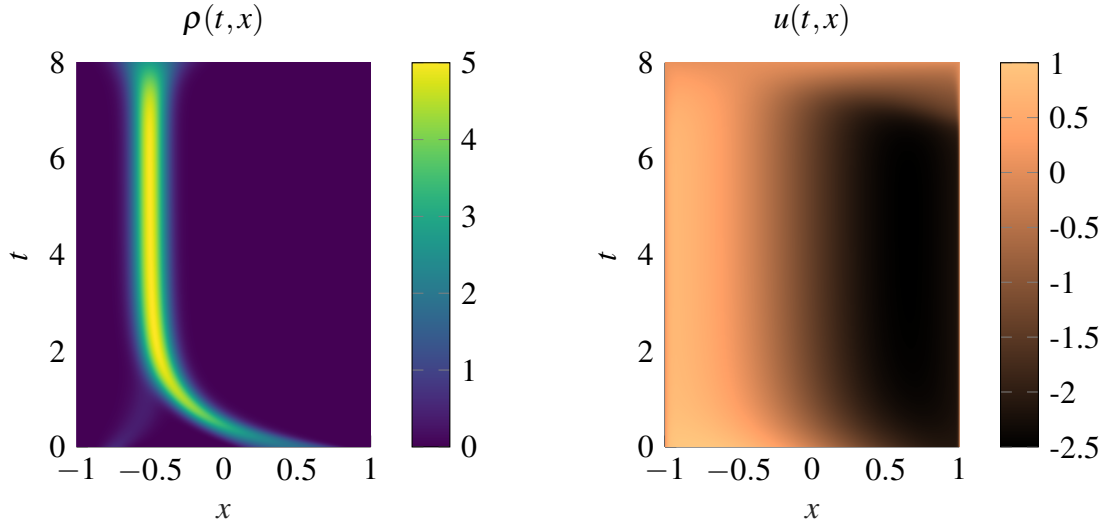

Figure 3: Evolution of the density $\rho(t,x)$ (left) and of the control $u(t,x)$ (right) up to the final time $T = 8$ for the Sznajd model described in Section 4.1.1 with $n = 800$ spatial discretization points and $m = 200$ time steps.

4.1.2 Hegselmann–Krause model

In the second numerical experiment we present an example of Hegselmann–Krause model for opinion formation taken from Reference [7]. In particular, we take the interaction function $p(x,y) = \chi_{\{|x-y|\leq\kappa\}}(x,y)$, with $\kappa = 0.15$, and the target point in the running cost $x_d = 0$. Moreover, we set the penalization parameter $\gamma = 2.5$ and the diffusion coefficient $\sigma = \sqrt{0.002}$. The initial density function is

$$\rho_0(x) = C(0.5 + \varepsilon(1 - x^2)),$$

where $\varepsilon = 0.01$ and C defined so that $\int_\Omega \rho_0(x)dx = 1$. For this model, we directly present the results using a spatial discretization of $n = 1000$ points and $m = 100$ time steps up to the final time $T = 10$. In Figures 5 and 6 we display the evolution of the density $\rho(t,x)$ and of the control $u(t,x)$. Similarly to the Sznajd model, the results match both the expectations and the outcomes in the literature. Then, we display in Figure 7 the value of the functional $\mathscr{J}(u^\ell)$ at the successive iterations of the steepest descent method. We observe that the method needs 15

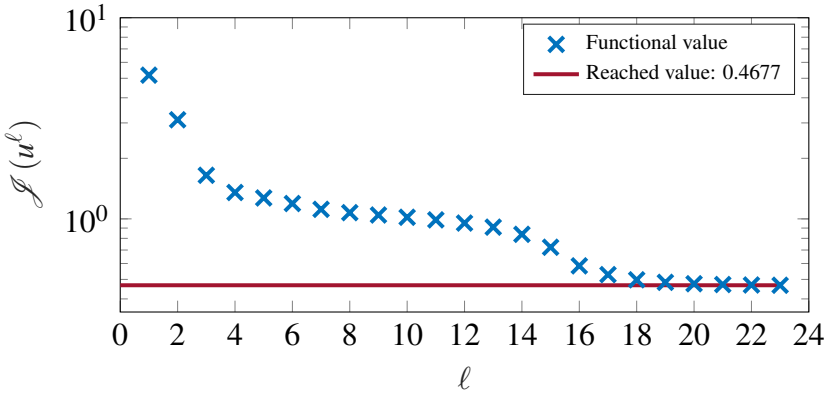

Figure 4: Value of the functional $\mathscr{J}(u^\ell)$ at the successive iterations of the steepest descent method for the Sznajd model described in Section 4.1.1 ($n = 800$ and $m = 200$).

iterations to reach the input tolerance $2 \cdot 10^{-3}$. Finally, this simulation takes roughly 15 seconds to run.

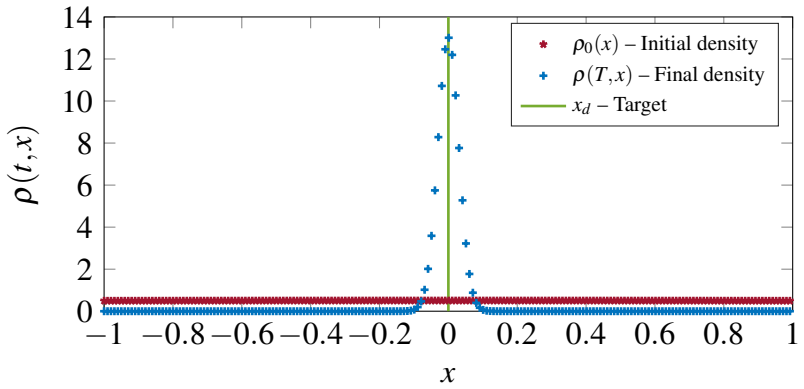

Figure 5: Density functions at initial time and at final time for the Hegselmann–Krause model described in Section 4.1.2 with $n = 1000$ spatial discretization points and $m = 100$ time steps. For visualization reasons, the densities are displayed each fifth point.

4.2 Crowd dynamics: fast exit scenario

In this section we consider a model for crowd dynamics taken from Reference [16]. We set the model in the spatial domain $\Omega = [-1,1]$, whose boundaries represent the exit doors. The non-local interaction kernel $p(x,y)$ is null and the selective function $s(t,x,\rho)$ is $1-\rho$ (hence, we employ the exponential Euler method (12) for the forward equation). The diffusion parameter is $\sigma = \sqrt{0.04}$, the exit intensity flux is $\beta = 10$, the penalization parameter is $\gamma = 1$, and the running cost is $e(t,x,\rho) = \rho$. The initial density function models the presence of two distinct groups, namely $\rho_0(x) = 0.9\mathrm{e}^{-100(x+0.4)^2} + 0.65\mathrm{e}^{-150x^2}$.

Similarly to the opinion dynamics case, we first show that the expected temporal rate of convergence of the exponential integrators is preserved after a complete solution of the model. To this purpose, we discretize this problem with $n = 200$ spatial discretization points and with different number of time steps, from $m = 300$ to $m = 700$, up to the final time $T = 2$. After the stabilization of the functional $\mathscr{J}$ in the steepest descent algorithm, we measure the error at

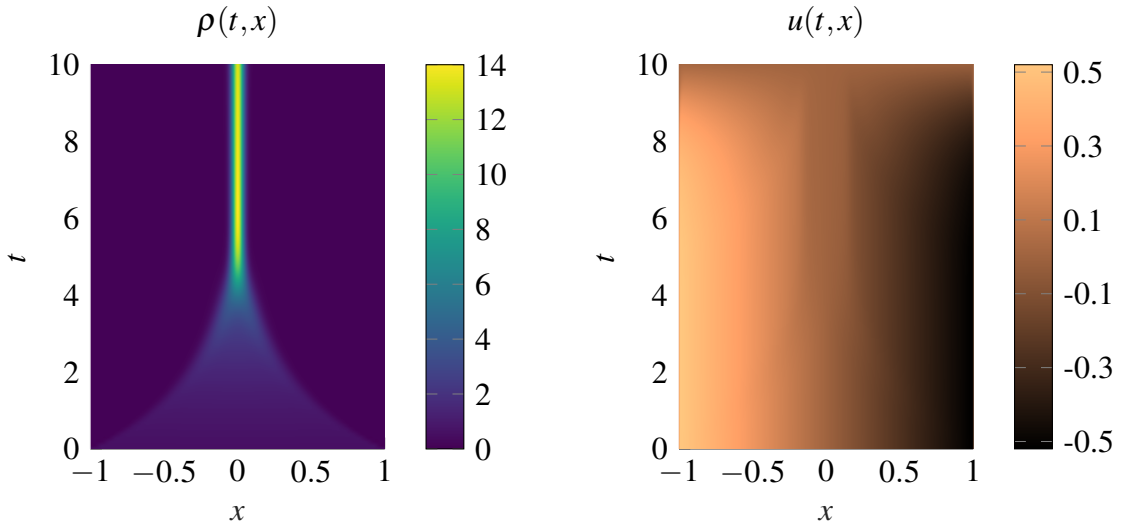

Figure 6: Evolution of the density $\rho(t,x)$ (left) and of the control $u(t,x)$ (right) up to the final time $T = 10$ for the Hegselmann–Krause model described in Section 4.1.2 with $n = 1000$ spatial discretization points and $m = 100$ time steps.

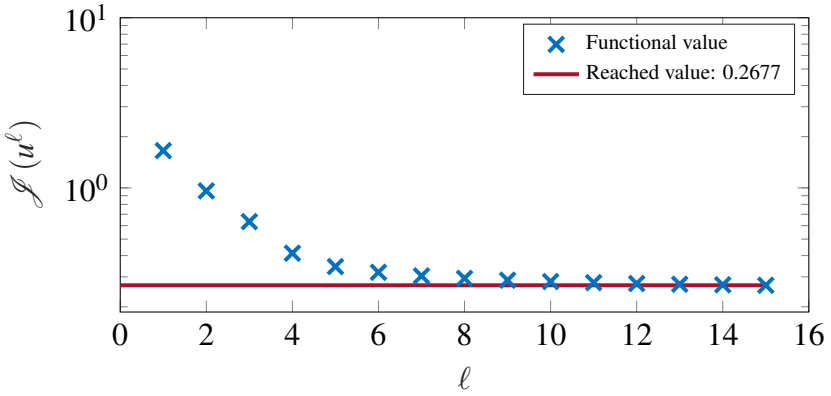

Figure 7: Value of the functional $\mathscr{J}(u^\ell)$ at the successive iterations of the steepest descent method for the Hegselmann–Krause model described in Section 4.1.2 ($n = 1000$ and $m = 100$).

final time for $\boldsymbol{\rho}(t)$ and at initial time for $\boldsymbol{\psi}(t)$ with respect to reference solutions. We display in Figure 8 the obtained relative errors which again confirm the expected accuracy and rate of convergence.

Then, we solve the same model up to the final time $T = 3$ and show its behavior. We discretize this problem with $n = 1000$ spatial discretization points and $m = 250$ time steps. We show the evolution of the density and of the control in Figures 9 and 10, where we can clearly see the exit of the crowd from the two doors. Moreover, we show in Figure 11 the value of the functional $\mathscr{J}(u^\ell)$ at the successive iterations of the steepest descent method. We observe that the method needs 13 iterations to reach the input tolerance $2 \cdot 10^{-3}$. Finally, the overall computational time of this simulation is about 45 seconds.

4.3 Mass transfer problem via optimal control

In this final example, we present an optimal control approach to a mass transfer problem, see for instance References [13, 51], where the particle density accounts for non-local interactions [14,

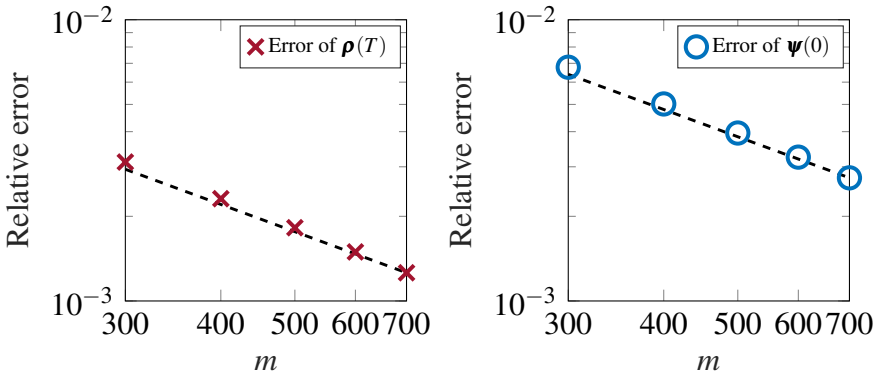

Figure 8: Relative errors in the infinity norm of $\boldsymbol{\rho}(T)$ ($T = 2$, left plot) and $\boldsymbol{\psi}(0)$ (right plot), with respect to a reference solution, for the pedestrian model described in Section 4.2 with $n = 200$ spatial discretization points and varying number of time steps m. A black dashed reference line of slope -1 is also displayed.

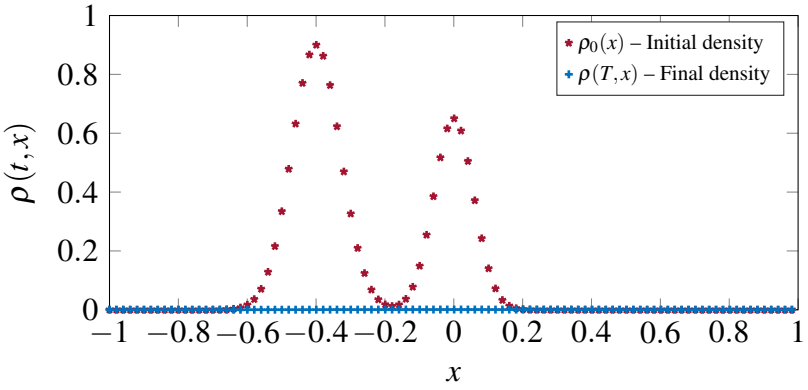

Figure 9: Density functions at initial time and at final time for the two-group crowd model described in Section 4.2 with $n = 1000$ spatial discretization points and $m = 250$ time steps. For visualization reasons, the densities are displayed each tenth point.

25]. Hence, the goal is to move the initial density function in the spatial domain $\Omega = [-1,1]$

$$\rho_0(x) = Ce^{-(x-\mu_0)^2/(2\sigma_0^2)},$$

where $\mu_0 = 0$, $\sigma_0 = 0.1$, and C is defined so that $\int_\Omega \rho_0(x)dx = 1$, to a target one

$$\bar{\rho}(x) = \bar{C}\left(e^{-(x-\mu_1)^2/(2\sigma_1^2)} + e^{-(x-\mu_2)^2/(2\sigma_2^2)}\right),$$

where $\mu_1 = 0.5$, $\sigma_1 = 0.1$, $\mu_2 = -0.3$, and $\sigma_2 = 0.15$, and $\bar{C}$ is defined so that $\int_\Omega \bar{\rho}(x)dx = 1$. The boundary conditions are of zero-flux type, the running cost is $e(t,x,\rho) = (\rho - \bar{\rho})^2$, the interaction kernel is of Sznajd type $p(x,y) = (x^2-1)/20$, and the selective function is $s(t,x,\rho) = 1$. The penalization parameter is $\gamma = 0.1$ and the diffusion parameter is $\sigma = \sqrt{0.02}$. We discretize the problem with $n = 1000$ spatial grid points and $m = 200$ time steps, and we run the simulation up to the final time $T = 3$. We consider a terminal cost given by $c(T,x,\rho(T,x)) = (\rho(T,x) - \bar{\rho}(x))^2$, which translates into $\psi_T(x) = \rho(T,x) - \bar{\rho}(x)$. In Figure 12 we plot the density functions at initial and final time, and we can observe that the initial density is correctly transported to the target one. In addition, in Figure 13 we present the evolution

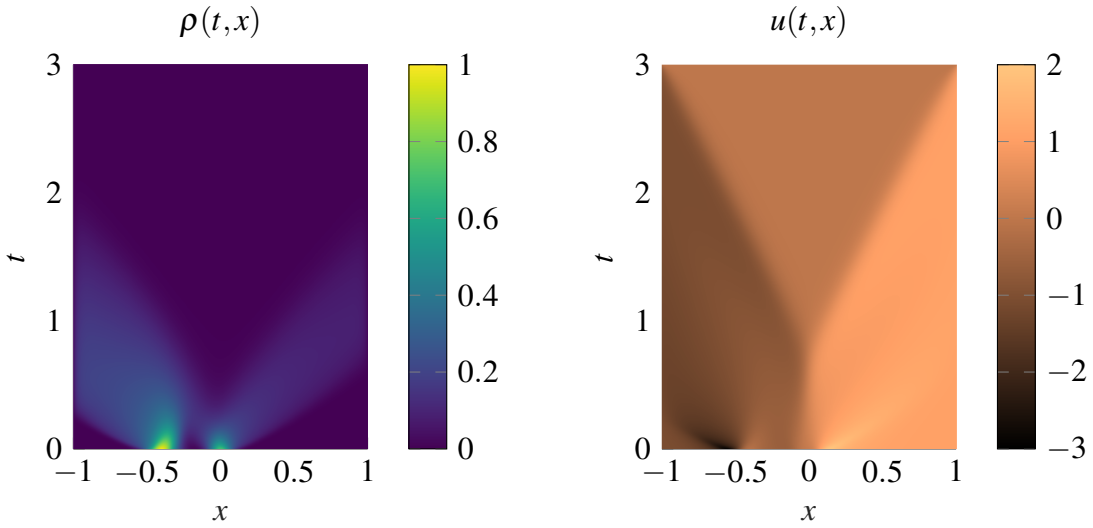

Figure 10: Evolution of the density $\rho(t,x)$ (left) and of the control $u(t,x)$ (right) up to the final time $T = 3$ for the two-group crowd model described in Section 4.2 with $n = 1000$ spatial discretization points and $m = 250$ time steps.

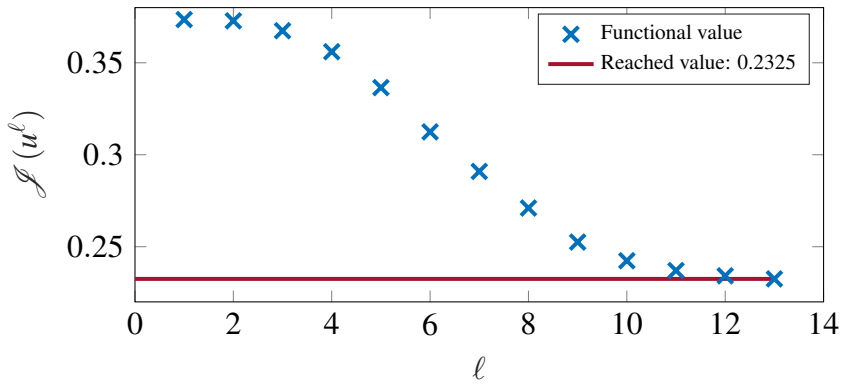

Figure 11: Value of the functional $\mathscr{J}(u^\ell)$ at the successive iterations of the steepest descent method for the two-group crowd model described in Section 4.2 ($n = 1000$ and $m = 250$).

of the density and of the control. Finally, we show in Figure 14 the values of the functional $\mathscr{J}(u^\ell)$ at the successive iterations of the steepest descent method. We observe that the method needs 33 iterations to reach the input tolerance $2 \cdot 10^{-3}$, with an overall computational time of this simulation of roughly 75 seconds.

5 Conclusions

We presented a mean-field optimal control model where the constraint is represented by a non-linear PDE with non-local interaction term and diffusion describing the evolution of a continuum of agents. We provide, at a formal level, first order optimality conditions, resulting in a forward–backward coupled system with associated boundary conditions. Thus, a reduced gradient method is derived for the synthesis of the mean-field control, where the primal and adjoint equations are efficiently solved by using exponential integrators. Our proposed approach has been successfully tested on various examples from the literature, including models of opinion formation and pedestrian dynamics in the one-dimensional setting. In future works we

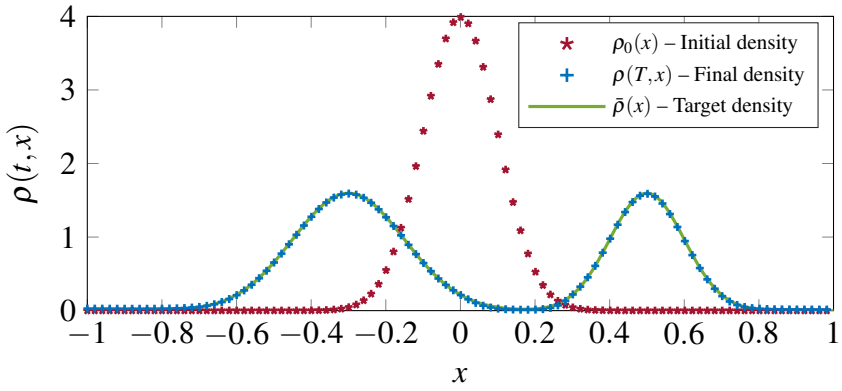

Figure 12: Density functions at initial time and at final time for the mass transfer problem described in Section 4.3 with $n = 1000$ spatial discretization points and $m = 200$ time steps.

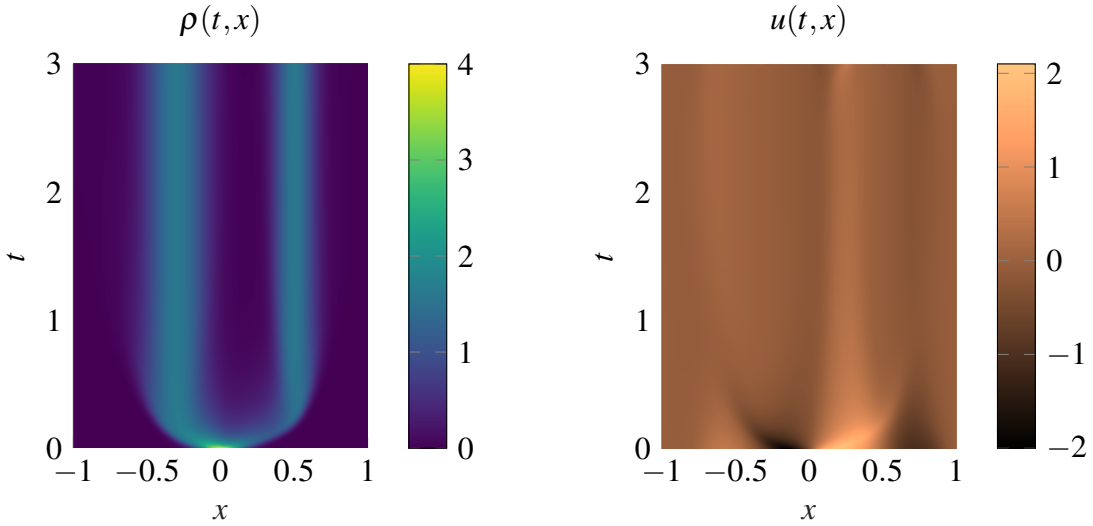

Figure 13: Evolution of the density $\rho(t,x)$ (left) and of the control $u(t,x)$ (right) up to the final time $T = 3$ for the mass transfer problem described in Section 4.3 with $n = 1000$ spatial discretization points and $m = 200$ time steps.

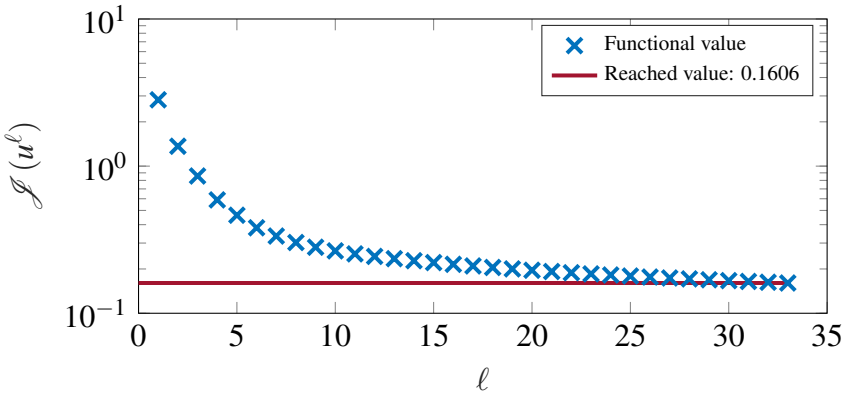

Figure 14: Value of the functional $\mathscr{J}(u^\ell)$ at the successive iterations of the steepest descent method for the mass transfer problem described in Section 4.3.

plan to exploit the efficiency of exponential integrators to tackle higher dimensional problems (possibly using ad hoc techniques for tensor structured problems [19, 20, 21]) and scenarios where a fine spatial discretization is required to correctly capture the behavior of the controlled dynamics.

Acknowledgments

The authors are members of the INdAM group GNCS, and acknowledge the support of the Italian Ministry of University and Research (MUR) through the MUR-PRIN Project 2022 No. 2022N9BM3N "Efficient numerical schemes and optimal control methods for time-dependent partial differential equations" and MUR-PRIN Project 2022 PNRR (No. P2022JC95T) "Data-driven discovery and control of multi-scale interacting artificial agent systems", financed by the European Union - Next Generation. Fabio Cassini holds a post-doc fellowship funded by INdAM.

The authors are former colleagues of Professor Leonard Peter Bos, and they would like to express their gratitude for his valuable presence in the Department of Computer Science at the University of Verona and all his precious advice.

Declaration of interests

The authors declare that they have no known competing financial interests or personal relationships that could have appeared to influence the work reported in this paper.

References

[1] Y. Achdou and I. Capuzzo-Dolcetta. Mean Field Games: Numerical Methods. *SIAM J. Numer. Anal.*, 48(3):1136–1162, 2010. URL https://doi.org/10.1137/090758477.

[2] M. Aduamoah, B. D. Goddard, J. W. Pearson, and J. C. Roden. Pseudospectral methods and iterative solvers for optimization problems from multiscale particle dynamics. *BIT Numer. Math.*, 62:1703–1743, 2022. URL https://doi.org/10.1007/s10543-022-00928-w.

[3] A. H. Al-Mohy and N. J. Higham. A New Scaling and Squaring Algorithm for the Matrix Exponential. *SIAM J. Matrix Anal. Appl.*, 31(3):970–989, 2009. URL https://doi.org/10.1137/09074721X.

[4] A. H. Al-Mohy and N. J. Higham. Computing the Action of the Matrix Exponential with an Application to Exponential Integrators. *SIAM J. Sci. Comput.*, 33(2):488–511, 2011. URL https://doi.org/10.1137/100788860.

[5] G. Albi, M. Herty, and L. Pareschi. Kinetic description of optimal control problems and applications to opinion consensus. *Commun. Math. Sci.*, 13(6):1407–1429, 2015. URL https://doi.org/10.4310/CMS.2015.v13.n6.a3.

[6] G. Albi, M. Bongini, E. Cristiani, and D. Kalise. Invisible Control of Self-Organizing Agents Leaving Unknown Environments. *SIAM J. Appl. Math.*, 76(4):1683–1710, 2016. URL https://doi.org/10.1137/15M1017016.

[7] G. Albi, Y.-P. Choi, M. Fornasier, and D. Kalise. Mean Field Control Hierarchy. *Appl. Math. Optim.*, 76:93–135, 2017. URL https://doi.org/10.1007/s00245-017-9429-x.

[8] G. Albi, N. Bellomo, L. Fermo, S.-Y. Ha, J. Kim, L. Pareschi, D. Poyato, and J. Soler. Vehicular traffic, crowds, and swarms: From kinetic theory and multiscale methods to applications and research perspectives. *Math. Models Methods Appl. Sci.*, 29(10):1901–2005, 2019. URL https://doi.org/10.1142/S0218202519500374.

[9] G. Albi, M. Herty, and L. Pareschi. Linear multistep methods for optimal control problems and applications to hyperbolic relaxation systems. *Appl. Math. Comput.*, 354:460–477, 2019. URL https://doi.org/10.1016/j.amc.2019.02.021.

[10] G. Albi, F. Ferrarese, and C. Segala. Optimized leaders strategies for crowd evacuation in unknown environments with multiple exits. In *Crowd Dynamics, Volume 3: Modeling and Social Applications in the Time of COVID-19*, Modeling and Simulation in Science, Engineering and Technology, pages 97–131. Birkhäuser, Cham, 2021. URL https://doi.org/10.1007/978-3-030-91646-6_5.

[11] G. Albi, S. Almi, M. Morandotti, and F. Solombrino. Mean-field selective optimal control via transient leadership. *Appl. Math. Optim.*, 85:22, 2022. URL https://doi.org/10.1007/s00245-022-09837-4.

[12] R. Bailo, M. Bongini, J. A. Carrillo, and D. Kalise. Optimal consensus control of the Cucker-Smale model. *IFAC-PapersOnLine*, 51(13):1–6, 2018. URL https://doi.org/10.1016/j.ifacol.2018.07.245.

[13] J.-D. Benamou and Y. Brenier. A computational fluid mechanics solution to the Monge-Kantorovich mass transfer problem. *Numer. Math.*, 84:375–393, 2000. URL https://doi.org/10.1007/s002110050002.

[14] M. Bongini and G. Buttazzo. Optimal control problems in transport dynamics. *Math. Models Methods Appl. Sci.*, 27(3):427–451, 2017. URL https://doi.org/10.1142/S0218202517500063.

[15] A. Borzì and V. Schulz. *Computational Optimization of Systems Governed by Partial Differential Equations*. Computational Science & Engineering. SIAM, Philadelphia, PA, 2011. URL https://doi.org/10.1137/1.9781611972054.

[16] M. Burger, M. Di Francesco, P. A. Markowich, and M.-T. Wolfram. On a mean field game optimal control approach modeling fast exit scenarios in human crowds. In *52nd IEEE Conference on Decision and Control*, pages 3128–3133, 2013. URL https://doi.org/10.1109/CDC.2013.6760360.

[17] M. Burger, R. Pinnau, C. Totzeck, and O. Tse. Mean-Field Optimal Control and Optimality Conditions in the Space of Probability Measures. *SIAM J. Control Optim.*, 59(2):977–1006, 2021. URL https://doi.org/10.1137/19M1249461.

[18] M. Caliari and F. Zivcovich. On-the-fly backward error estimate for matrix exponential approximation by Taylor algorithm. *J. Comput. Appl. Math.*, 346:532–548, 2019. URL https://doi.org/10.1016/j.cam.2018.07.042.

[19] M. Caliari, F. Cassini, L. Einkemmer, A. Ostermann, and F. Zivcovich. A μ-mode integrator for solving evolution equations in Kronecker form. *J. Comput. Phys.*, 455:110989, 2022. URL https://doi.org/10.1016/j.jcp.2022.110989.

[20] M. Caliari, F. Cassini, and F. Zivcovich. A μ-mode BLAS approach for multidimensional tensor-structured problems. *Numer. Algorithms*, 92(4):2483–2508, 2023. URL https://doi.org/10.1007/s11075-022-01399-4.

[21] M. Caliari, F. Cassini, and F. Zivcovich. A μ-mode approach for exponential integrators: actions of φ-functions of Kronecker sums. *Calcolo*, 2024. URL https://doi.org/10.1007/s10092-024-00610-3. Accepted for publication.

[22] P. Cannarsa, R. Capuani, and P. Cardaliaguet. Mean field games with state constraints: from mild to pointwise solutions of the PDE system. *Calc. Var. Partial Diff. Equ.*, 60:108, 2021. URL https://doi.org/10.1007/s00526-021-01936-4.

[23] M. Caponigro, M. Fornasier, B. Piccoli, and E. Trélat. Sparse stabilization and control of alignment models. *Math. Models Methods Appl. Sci.*, 25(3):521–564, 2015. URL https://doi.org/10.1142/S0218202515400059.

[24] R. Carmona and M. Laurière. Convergence analysis of machine learning algorithms for the numerical solution of mean field control and games: II—the finite horizon case. *Ann. Appl. Probab.*, 32(6):4065–4105, 2022. URL https://doi.org/10.1214/21-AAP1715.

[25] J. A. Carrillo, M. Di Francesco, A. Figalli, T. Laurent, and D. Slepčev. Confinement in nonlocal interaction equations. *Nonlinear Anal. Theory Methods Appl.*, 75(2):550–558, 2012. URL https://doi.org/10.1016/j.na.2011.08.057.

[26] Y.-P. Choi, D. Kalise, J. Peszek, and A. A. Peters. A Collisionless Singular Cucker–Smale Model with Decentralized Formation Control. *SIAM J. Appl. Dyn. Syst.*, 18(4):1954–1981, 2019. URL https://doi.org/10.1137/19M1241799.

[27] E. Cristiani, B. Piccoli, and A. Tosin. *Multiscale Modeling of Pedestrian Dynamics*, volume 12 of *Modeling, Simulation & Applications*. Springer, Cham, 2014. URL https://doi.org/10.1007/978-3-319-06620-2.

[28] F. Cucker and S. Smale. Emergent Behavior in Flocks. *IEEE Trans. Automat. Control*, 52(5):852–862, 2007. URL https://doi.org/10.1109/TAC.2007.895842.

[29] P. Degond, J.-G. Liu, S. Motsch, and V. Panferov. Hydrodynamic models of self-organized dynamics: Derivation and existence theory. *Methods Appl. Anal.*, 20(2):89–114, 2013. URL https://doi.org/10.4310/MAA.2013.v20.n2.a1.

[30] M. R. D'Orsogna, Y. L. Chuang, A. L. Bertozzi, and L. S. Chayes. Self-Propelled Particles with Soft-Core Interactions: Patterns, Stability, and Collapse. *Phys. Rev. Lett.*, 96(10):104302, 2006. URL https://link.aps.org/doi/10.1103/PhysRevLett.96.104302.

[31] J. R. G. Dyer, A. Johansson, D. Helbing, I. D. Couzin, and J. Krause. Leadership, consensus decision making and collective behaviour in humans. *Philos. Trans. R. Soc. B*, 364(1518):781–789, 2009. URL https://doi.org/10.1098/rstb.2008.0233.

[32] M. Fornasier and F. Solombrino. Mean-Field Optimal Control. *ESAIM Control Optim. Calc. Var.*, 20(4):1123–1152, 2014. URL https://doi.org/10.1051/cocv/2014009.

[33] M. Fornasier, B. Piccoli, and F. Rossi. Mean-field sparse optimal control. *Philos. Trans. R. Soc. A*, 372(2028):20130400, 2014. URL https://doi.org/10.1098/rsta.2013.0400.

[34] G. Freudenthaler and T. Meurer. PDE-based multi-agent formation control using flatness and backstepping: Analysis, design and robot experiments. *Automatica*, 115:108897, 2020. URL https://doi.org/10.1016/j.automatica.2020.108897.

[35] S. Gaudreault, G. Rainwater, and M. Tokman. KIOPS: A fast adaptive Krylov subspace solver for exponential integrators. *J. Comput. Phys.*, 372:236–255, 2018. URL https://doi.org/10.1016/j.jcp.2018.06.026.

[36] J. Gómez-Serrano, C. Graham, and J.-Y. Le Boudec. The bounded confidence model of opinion dynamics. *Math. Models Methods Appl. Sci.*, 22(2):1150007, 2012. URL https://doi.org/10.1142/S0218202511500072.

[37] W. W. Hager. Runge-Kutta methods in optimal control and the transformed adjoint system. *Numer. Math.*, 87:247–282, 2000. URL https://doi.org/10.1007/s002110000178.

[38] R. Hegselmann and U. Krause. Opinion dynamics and bounded confidence models, analysis, and simulation. *J. Artif. Soc. Soc. Simul.*, 5(3), 2002. URL http://jasss.soc.surrey.ac.uk/5/3/2.html.

[39] M. Herty and L. Pareschi. Fokker-Planck asymptotics for traffic flow models. *Kinet. Relat. Models*, 3(1):165–179, 2010. URL https://doi.org/10.3934/krm.2010.3.165.

[40] M. Herty, L. Pareschi, and S. Steffensen. Implicit-Explicit Runge–Kutta Schemes for Numerical Discretization of Optimal Control Problems. *SIAM J. Numer. Anal.*, 51(4):1875–1899, 2013. URL https://doi.org/10.1137/120865045.

[41] M. Hochbruck and A. Ostermann. Exponential integrators. *Acta Numer.*, 19:209–286, 2010. URL https://doi.org/10.1017/S0962492910000048.

[42] M. Huang, R. P. Malhamé, and P. E. Caines. Large population stochastic dynamic games: closed-loop McKean-Vlasov systems and the Nash certainty equivalence principle. *Commun. Inf. Syst.*, 6(3):221–252, 2006. URL http://projecteuclid.org/euclid.cis/1183728987.

[43] J. M. Lasry and P. L. Lions. Mean field games. *Japanese J. Math.*, 2:229–260, 2007. URL https://doi.org/10.1007/s11537-007-0657-8.

[44] V. T. Luan, J. A. Pudykiewicz, and D. R. Reynolds. Further development of efficient and accurate time integration schemes for meteorological models. *J. Comput. Phys.*, 376:817–837, 2019. URL https://doi.org/10.1016/j.jcp.2018.10.018.

[45] S. Motsch and E. Tadmor. Heterophilious Dynamics Enhances Consensus. *SIAM Rev.*, 56(4):577–621, 2014. URL https://doi.org/10.1137/120901866.

[46] K.-K. Oh, M.-C. Park, and H.-S. Ahn. A survey of multi-agent formation control. *Automatica*, 53:424–440, 2015. URL https://doi.org/10.1016/j.automatica.2014.10.022.

[47] A. A. Peters, R. H. Middleton, and O. Mason. Leader tracking in homogeneous vehicle platoons with broadcast delays. *Automatica*, 50(1):64–74, 2014. URL https://doi.org/10.1016/j.automatica.2013.09.034.

[48] B. Piccoli and A. Tosin. Pedestrian flows in bounded domains with obstacles. *Continuum Mech. Thermodyn.*, 21(2):85–107, 2009. URL https://doi.org/10.1007/s00161-009-0100-x.

[49] L. Ruthotto, S. J. Osher, W. Li, L. Nurbekyan, and S. W. Fung. A machine learning framework for solving high-dimensional mean field game and mean field control problems. *Proc. Natl. Acad. Sci. U.S.A.*, 117(17):9183–9193, 2020. URL https://doi.org/10.1073/pnas.1922204117.

[50] Y. Saad. Analysis of Some Krylov Subspace Approximations to the Matrix Exponential Operator. *SIAM J. Numer. Anal.*, 29(1):209–228, 1992. URL https://doi.org/10.1137/0729014.

[51] F. Santambrogio. *Optimal Transport for Applied Mathematicians: Calculus of Variations, PDEs, and Modeling*, volume 87 of *Progress in Nonlinear Differential Equations and Their Applications*. Birkhäuser, Cham, 2015. URL https://doi.org/10.1007/978-3-319-20828-2.

[52] J. Sastre, J. Ibáñez, and E. Defez. Boosting the computation of the matrix exponential. *Appl. Math. Comput.*, 340:206–220, 2019. URL https://doi.org/10.1016/j.amc.2018.08.017.

[53] B. Skaflestad and W. M. Wright. The scaling and modified squaring method for matrix functions related to the exponential. *Appl. Numer. Math.*, 59(3–4):783–799, 2009. URL https://doi.org/10.1016/j.apnum.2008.03.035.

[54] K. Sznajd-Weron and J. Sznajd. Opinion evolution in closed community. *Int. J. Mod. Phys. C*, 11(6):1157–1165, 2000. URL https://doi.org/10.1142/S0129183100000936.

[55] G. Toscani. Kinetic models of opinion formation. *Commun. Math. Sci.*, 4(3):481–496, 2006. URL http://projecteuclid.org/euclid.cms/1175797553.